IRAQI JOURNAL OF APPLIED PHYSICS
Vol. 22, No. 3, July-September 2026, pp. 393-406

Malik J. Hussein [1,3*]
Wa'il A.G. Al-Tumah [1]
Ahmad H. AL-Shaheen [2]

[1] Department of Physics, College of Science, University of Basrah, Basrah, IRAQ
[2] Department of Physics, College of Science, University of Misan, Misan, IRAQ
[3] General Directorate of Education in Muthanna, Ministry of Education, Muthanna, IRAQ
*Corresponding author Email: pgs.malik.jasim@uobasrah.edu.iq

Semi-Empirical Equation for a Semi-Circular PIFA

This article introduces a newly proposed Equation for the calculation of the optimal radius of the semicircular structure of the Planar Inverted-F Antenna (PIFA), derived by equating the area of the equivalent rectangular structure and the area of the given structure. The Equation was tested using HFSS simulation at operating frequencies of 2.4 GHz, 5.2 GHz, and 5.8 GHz with substrate materials of relative permittivity 2.55, 3.2, and 4.4. To further examine the Equation's reliability under practical scenarios, three antenna prototypes were implemented on the FR4 substrate (ε_r = 4.4) at the same frequencies. The measured S11 showed clear resonance minima at the corresponding operating frequencies that matched the theoretical values and simulation results. The strong agreement of the theoretical results with the simulation results and the experimentally measured results, supported by a Pearson's correlation coefficient of 0.999, validates the proposed Equation's usability for designing a compact semicircular PIFA structure.

Keywords: Planar inverted-F antenna; HFSS; Mobile communications; Specific absorption rate
Received: 12 September 2025; Revised: 7 December; Accepted: 14 December; Published: 1 July 2026

1. Introduction

Over the recent years, wireless and mobile communication technologies have been developed significantly. This rapid growth has been stimulated by the growing demand for higher data speeds combined with smaller and more portable devices, and good connectivity across a wide range of environments. A major element at the core of such systems is the antenna, which has a vital role in deciding the performance of a device, its efficiency, and how easily it could be mingled into compact modern designs. As a result, antennas received great attention of research, especially as the requirements for advanced generation systems such as 3G, 4G, and the emergence of 5G networks continue to evolve [1-5].

Since wireless devices have become more complex and multifunctional, the need for small, efficient, and multiband antennas which could be placed in limited space has grown significantly. Increasing demand for integration of several functions in a single portable device while still considering user requirements and safety has had a great impact on antenna design. Factors such as device ergonomics, the amount by which the antenna is closed to the user's body, and their compliance to standards of SAR assume critical roles in the design considerations [6-8].

In addition, it has become clearer that user interactions with portable devices could highly affect antenna performance, usually causing signal detuning or reduced efficiency because of the close presence of the human body [9-11]. This complexity has led to a shift in the way antennas are integrated into portable devices, shifting away from external, extendable designs toward smaller, embedded antennas. During the 1980s, monopole antennas had been used in mobile phones because of their omnidirectional radiation patterns [12]. Nevertheless, since mobiles have become smaller and more evolved, the large size of monopole antennas classified them as less practical. Addressing this, several low-profile alternatives have been developed. One of these designs was the Inverted-L Antenna (ILA), which uses short vertical section combined with a longer horizontal arm running parallel to the ground plane. Although ILA offers a lower profile, it meets some difficulties in impedance matching due to its low radiation resistance and high capacitive reactance especially caused by the horizontal segment being very close to the ground. In order to overcome these limitations, the Inverted-F Antenna (IFA) has been introduced. By adding an L-shaped stub near the feed point, IFA helped to improve impedance matching by offering better control of the resonant path [13]. Though this design treated some issues solved some problems, it still suffers from a limited bandwidth due to its electrically small radiating elements. To solve this, the Planar Inverted-F Antenna (PIFA) is developed as a more evolved solution for mobile applications [14]. The PIFA features a flat radiating patch that is connected to the ground plane using a shorting pin or plate, and it is powered by a carefully placed feed point. Its design resembles an upside-down letter "F" [15]. This has improved the bandwidth, reduced the antenna's height, and made it easier to combine into compact devices. Due to its planar structure, the PIFA is also mechanically strong and could be produced without great difficulty by means of

the standard PCB techniques. In addition, it shows some support towards it that supports multiple frequency bands through design enhancements like implementing extra resonating structures or parasitic elements at the open end [16-18].

In addition to its structural benefits, PIFAs are useful in personal communication systems in particular where limiting radiation toward the user's head is important. Unlike monopole or whip antennas, which radiate equally in all directions, PIFAs reduces backward radiation. This does not improve overall efficiency only but also reduces the user's exposure to electromagnetic energy. Therefore, PIFAs are widely used now in smartphones, tablets, wearable devices, and a variety of wireless communication systems including the Internet of Things (IoT) [19]. As wireless technology seeks for better performance, higher data throughput, and smaller device footprints, PIFA is currently a central solution in antenna design relevant to both academic research as well as commercial applications.

Conventional circular and rectangular PIFAs have been widely researched and used because they are simple and work as expected. However, the semicircular PIFA has real benefits that solve specific design problems in small and conformal wireless devices. Recent studies, including [20,21], have shown that semicircular microstrip patches can reach the same resonant frequency as circular patches while taking up about 50% less space. This directly supports the miniaturization of antennas. The semicircular shape also has better radiation properties, such as a wider 3-dB beamwidth (≈107° vs 80°) and lower cross-polarization levels (≈32 dB isolation compared to 26 dB in circular patches). This makes it especially good for use on curved or space-limited surfaces in modern portable and wearable systems. These features show that the semicircular shape is not just a mathematical change, but a real improvement that makes polarization purity, radiation coverage, and spatial adaptability better than traditional circular and rectangular PIFAs.

The classical formulation of the dominant TM11 mode can be used to find the resonant frequency of a circular microstrip antenna. However, this Equation is only valid if the circular current distribution is perfectly symmetric. When the structure is changed to a semicircular shape, this symmetry is broken, which causes a small change in the distribution of the fringing field and the stored electromagnetic energy near the open edge. Table (I) in [20,21] shows that these asymmetries cause a measurable change in the resonant frequency (usually 0.02–0.05 GHz) when compared to the full circular case, even when the radii and substrate parameters are the same.

So, finding a separate closed-form equation for the semicircular configuration is not just a way to save time; it is also a necessary step to account for the boundary-dependent correction factors that come up because of the open periphery and smaller radiating aperture. The proposed equation provides a direct analytical tool to estimate the resonant frequency of semicircular patches without relying on empirical curve-fitting to the circular model, thus improving prediction accuracy and enabling faster optimization of compact antenna designs. In this sense, it contributes to the state-of-the-art by generalizing the classical circular model to asymmetric geometries that are increasingly relevant in miniaturized and conformal antenna systems[20,21].

2. Geometry of Antenna

In this research, we designed a semicircular PIFA, where the radius can be calculated using the circular antenna equation [22-24]:

$$a = \frac{F}{\sqrt{1+\frac{2h}{\pi\varepsilon_r F}\left[\ln\left(\frac{\pi F}{2h}+1.7726\right)\right]}} \quad (1)$$

where $F = \frac{8.791\times10^9}{f_r\sqrt{\varepsilon_r}}$, where a and ε_r represent the radius and dielectric constant of the circular microstrip antenna respectively and f_r resonant frequency given in GHz

However, an alternative method was employed to determine the radius by equating the area of the semicircle with the area of a rectangle [25]. Through this approach, we derived a semiempirical equation for calculating the radius of the semicircular PIFA. The resonant frequency of a PIFA is represented by the following formula[14,26,27]:

$$L_p + W_p - W_s + H = \frac{\lambda}{4\sqrt{\varepsilon_r}} = \frac{c}{4f_r\sqrt{\varepsilon_{reff}}} \quad (2)$$

$$\varepsilon_{reff} = \frac{\varepsilon_r+1}{2}$$

If $W_S = W_p$, equation (2) becomes as follows:

$$f_{rmax} = \frac{c}{4(L_p+H)\sqrt{\varepsilon_{reff}}} \quad (3)$$

As demonstrated in Fig. (1), the effective radius of a semicircular microstrip antenna can be computed by equating its area to that of a rectangular microstrip antenna [25]

$$A_{RMSA} = \frac{A_{SCMSA}}{2} \quad (4)$$

$$L \times W = \frac{\pi r^2}{2} \quad (5)$$

where L =2r

$$2r \times W = \frac{\pi r^2}{2}$$

$$W = \frac{\pi r}{4} \Leftrightarrow r = \frac{4w}{\pi} \quad (6)$$

From equations (3) and (6) can be found:

$$r = \frac{4}{\pi}\left(\frac{c}{4f_r\sqrt{\varepsilon_{eff}}} - H\right) = \frac{4}{\pi}\left(\frac{c}{4f_r\sqrt{\frac{\varepsilon_r+1}{2}}} - H\right) \quad (7)$$

To address the gap resulting from the resonant frequency between it and the circular shape equation (Eq. 1), a semi-empirical correction model was formulated on the basis of combined analytical and full-wave simulation data. First, the theoretical radius r was computed using Eq. (7) for a wide set of design conditions covering frequencies from 2.0 to 10 GHz and dielectric constants ε_r = 2.55, 3.2, 3.78, 4.0, 4.4, 5.5,

6.0. For each case, HFSS simulations were then performed, and the physical radius was iteratively adjusted until the target resonance was achieved (defined as $|S_{11}| \leq -10$ dB at the design frequency). This procedure yielded paired values (r, r_{HFSS}) representing the difference between the analytical prediction and the optimized electromagnetic result.

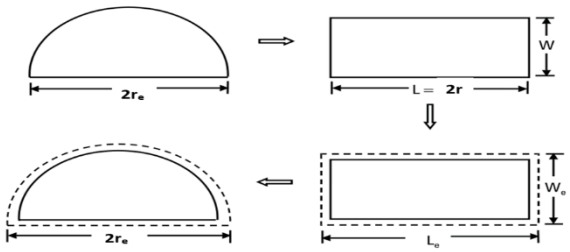

Fig. (1) Semicircular MSA and its equivalence to RMSA [25]

The complete dataset was fitted using several polynomial models (linear, quadratic, and cubic), and the quadratic form provided the best agreement, exhibiting the highest coefficient of determination R2 and the lowest root-mean-square error. The resulting semi-empirical expression is:

$$r_{eff} = 0.005\, r^2 + 0.57\, r + 2.3 \qquad (8)$$

where r is calculated from Eq. (7), and r_{eff} is the effective radius for use in the physical implementation to properly determine resonance within HFSS simulations

The quadratic term describes the nonlinearity introduced at both small and large radii because of fringing fields, ground planes, and dielectrics that are not fully accounted for the analytical equation. The linear term's coefficient continues to maintain the field's dominant behavior as described by theory, while another term (offset of 2.3 mm) adjusts for various systematic errors introduced because of substrate thickness, conductor and dielectric losses, as well as the feed and shorting strip's presence.

In Eq. (8), shows strong agreement with the classical circular patch formulation given by Eq. (1), but it is much simpler and more accurate for the semicircular PIFA geometry. Thus, it may be used to determine directly the required radius of a semicircular PIFA with enhanced reliability.

A semicircular PIFA as depicted in Fig. (2), will be designed with exact specifications by utilizing Eq. (8) to determine the radius r, which will be optimized for the chosen frequencies of 2.4 GHz, 5.2 GHz, and 5.8 GHz. For the structure to sustain the desired frequencies, the design will also take into consideration the substrate height (h), the strip width (w_s=2r), the base dimensions (l_g and w_g=2r), and the substrate height (h). The performance of the antenna will be assessed for a range of dielectric constants (ε_r) values: 2.55, 3.2, and 4.4, for each model. Table (1) displays antenna diameters at various frequencies and dielectric constants may be seen below.

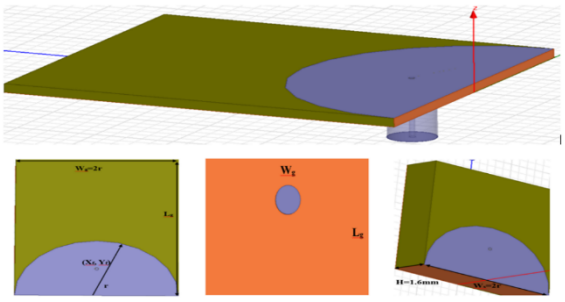

a-Top view *b-bottom view* *c- side view*

Fig. (2) The configuration of the proposed PIFA

3. Results and Discussion

In this section, the operation characteristics of the proposed antenna are examined, such as its return loss, gain, VSWR, input impedance and radiation pattern. HFSS electromagnetic simulation software was used to design and test the antenna. From the simulated return loss in Fig. (3), at ε_r= 2.55, there is clear resonance at 2.4 GHz with a minimum |S11| of less than -19.8 dB, which reflects excellent impedance matching at the frequency of operation. The corresponding VSWR shown in Fig. (4) is about 1.22 at resonance, again confirming the sufficiency of the matching bandwidth. As figure (5) shows, the input impedance converges to approximately 54 Ω, which is quite consistent with the conventional RF feeding networks.

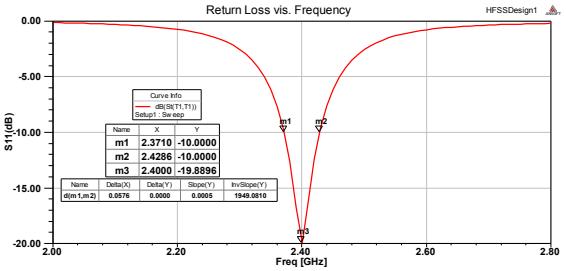

Fig. (3) Return Loss for the proposed antenna at 2.4 GHz, ε_r=2.55

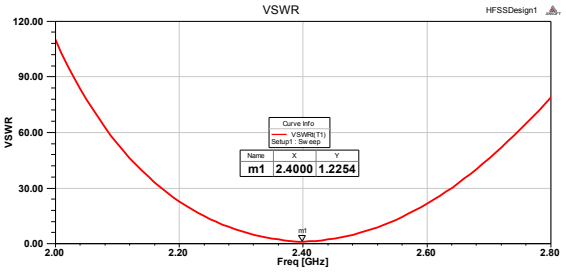

Fig. (4) VSWR for the proposed antenna at 2.4 GHz, ε_r=2.55

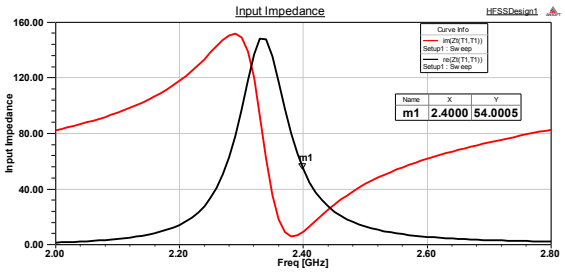

Fig. (5) Input Impedance for the proposed antenna at 2.4 GHz, ε_r=2.55

Moreover, figures (6) and (7) show the radiation performance, which has stable gain and directivity characteristics, reaching a peak in the directivity of about 5.3 dB. Figure (8) presents the 3D radiation pattern that confirms this result, with a well-defined main lobe and maximum realized gain of approximately 5.25 dB.

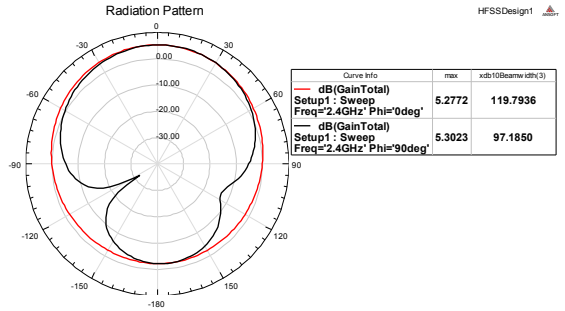

Fig. (6) 2D-Total gain for the proposed antenna at 2.4 GHz, ε_r=2.55

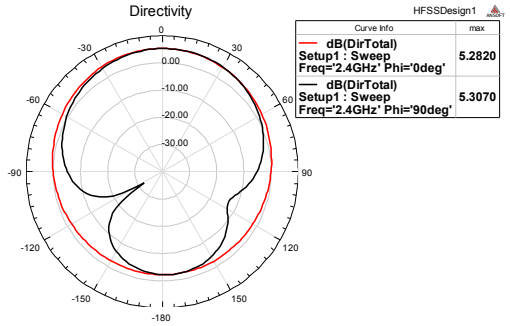

Fig. (7) 2D-Total Directivity for the proposed antenna at 2.4 GHz, ε_r=2.55

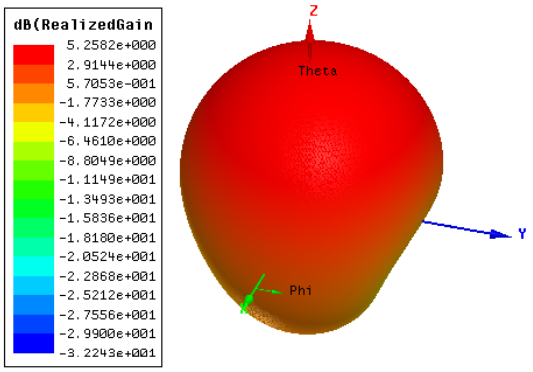

Fig. (8) 3D-Realized gain in dB for the proposed antenna at 2.4 GHz, ε_r=2.55

From Fig. (9), at ε_r= 3.2, the return loss shows a well-defined resonance at 2.4 GHz with a minimum |S11| value of −28.9 dB, which corroborates excellent impedance matching. For the same frequency, the corresponding VSWR in Fig. (10) reaches 1.07 within the resonant band, while the input impedance seen from Fig. (11) is about 46.57 Ω with minor reactive contributions, testifying to almost ideal matching conditions.

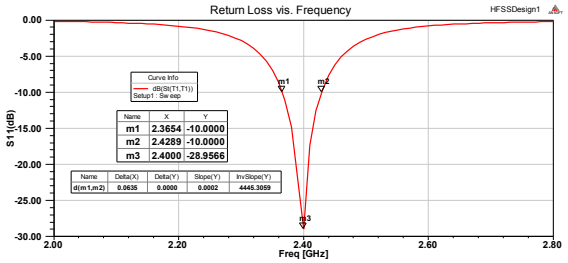

Fig. (9) Return Loss for the proposed antenna at 2.4 GHz, ε_r=3.2

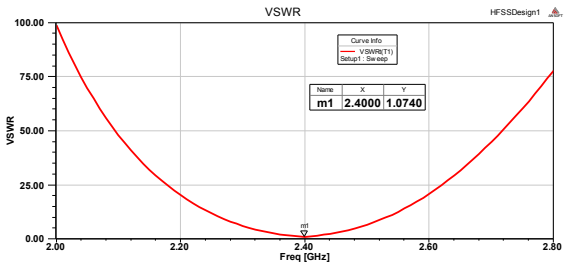

Fig. (10) VSWR for the proposed antenna at 2.4 GHz, ε_r=3.2

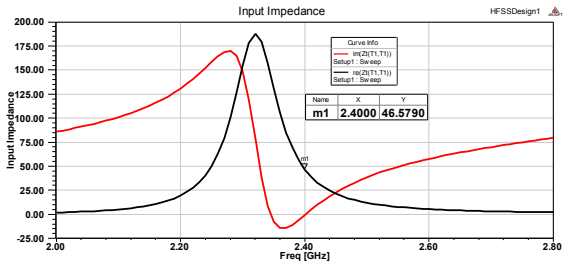

Fig. (11) Input Impedance for the proposed antenna at 2.4 GHz, ε_r=3.2

The radiation characteristics, as depicted in figures (12-14), reveal a stable and well-formed radiation distribution, although a slight degradation in peak performance compared to the lower-permittivity scenario is realized. The maximum directivity and realized gain are attained at 5.17 dB and 5.04 dB, respectively.

For ε_r =4.4, resonance occurs at approximately 2.4 GHz with a minimum return loss of −26.66 dB (Fig. 15). The VSWR is 1.09 at resonance (Fig. 16), and the input impedance (Fig. 17) is approximately 46.5 Ω, which implies slightly less than optimal matching compared to substrates with relatively lower values of permittivity.

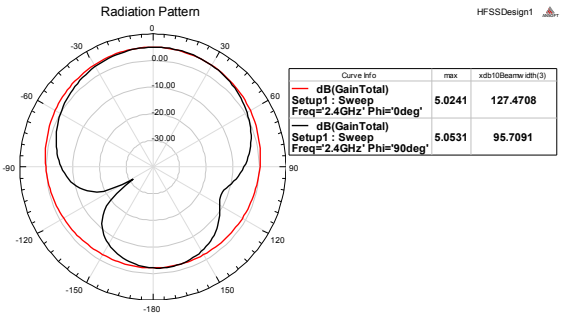

Fig. (12) 2D-Total gain for the proposed antenna at 2.4 GHz, ε_r=3.2

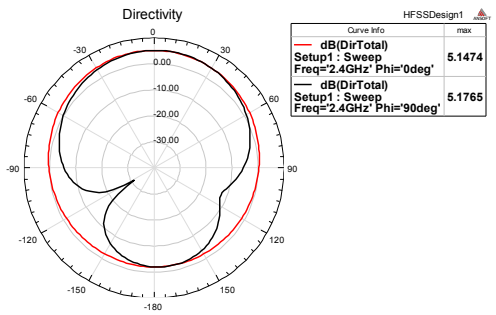

Fig. (13) 2D-Total Directivity for the proposed antenna at 2.4 GHz, ε_r=3.2

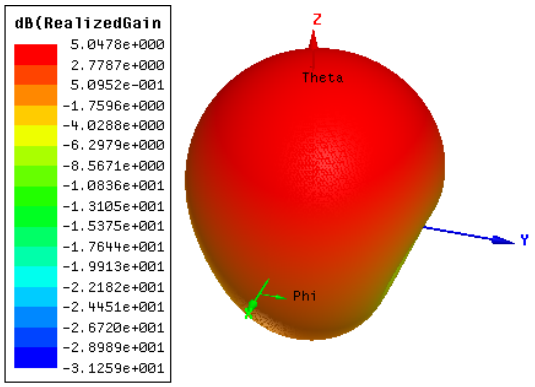

Fig. (14) 3D-Realized gain in dB for the proposed antenna at 2.4 GHz, ε_r=3.2

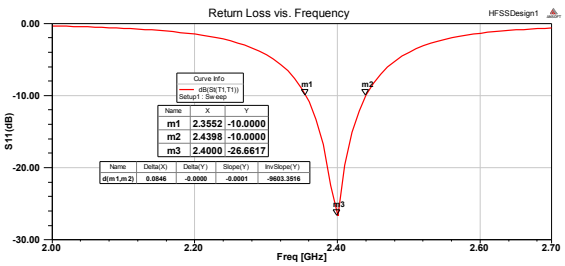

Fig. (15) Return Loss for the proposed antenna at 2.4 GHz, ε_r=4.4

The radiation characteristics presented in figures (18-20) show acceptable gain performance; however, a decrease in efficiency can be observed, which can be related to the higher dielectric losses usually inherent with FR4-like substrates. The maximum directivity and realized gain are noted as 5 dB and 3.01 dB, respectively.

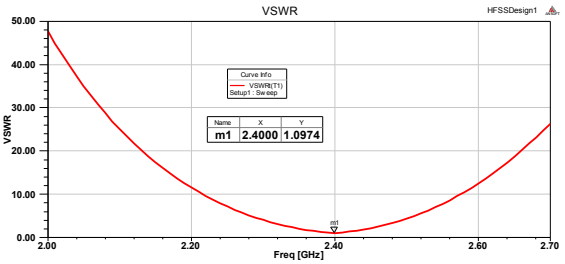

Fig. (16) VSWR for the proposed antenna at 2.4 GHz, ε_r=4.4

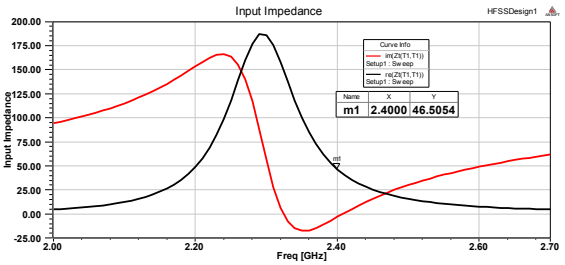

Fig. (17) Input Impedance for the proposed antenna at 2.4 GHz, ε_r=4.4

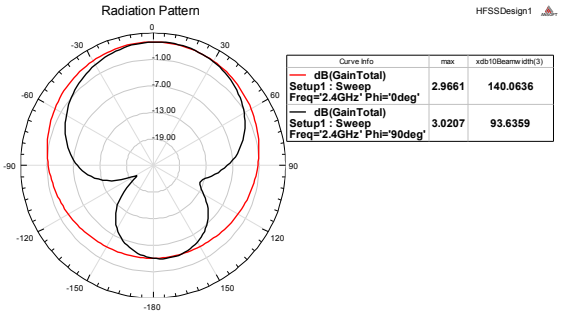

Fig. (18) 2D-Total gain for the proposed antenna at 2.4 GHz, ε_r=4.4

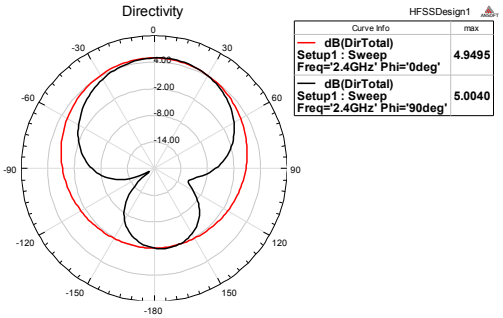

Fig. (19) 2D-Total Directivity for the proposed antenna at 2.4 GHz, ε_r=4.4

At 5.2 GHz with a relative permittivity of ε_r =2.55, the return loss |S11|, figure (21) presents a clear resonance at the same frequency with a value of around -20.5 dB, revealing an excellent impedance matching between the antenna and the feed line. The voltage standing wave ratio (VSWR) at resonance is 1.2, Fig. (22), while the input impedance, Fig. (23), is 60.36 Ω, reflecting a reasonably good matching condition.

The distribution of gain and directivity represented in figures (24-26) shows that the radiation pattern is broadside, with very high values for the two

parameters, which confirms that the antenna is highly efficient at this frequency. The maximum gain is 6.07dB, and the maximum directivity is 6.14 dB.

In the case of ε_r =3.2, the resonant frequency has remained at 5.2 GHz, where the resonance is very strong as |S11| (Fig. 27) reaches approximately -23.38 dB. The VSWR at resonance is 1.14 as shown by Fig. (28), while the input impedance in Fig. (29) is 43.9 Ω showing higher reactive components compared with the previous case.

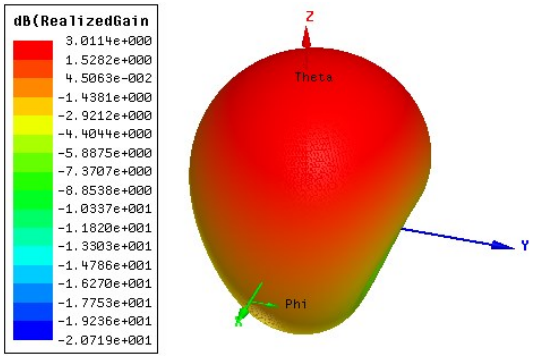

Fig. (20) 3D-Realized gain in dB for the proposed antenna at 2.4 GHz, ε_r=4.4

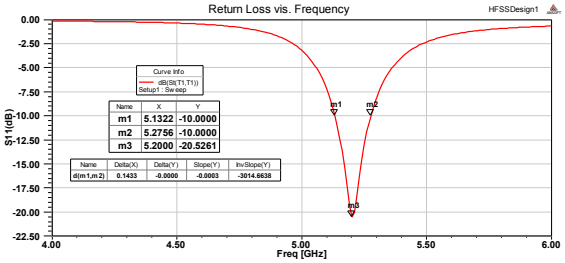

Fig. (21) Return Loss for the proposed antenna at 5.2 GHz, ε_r=2.55

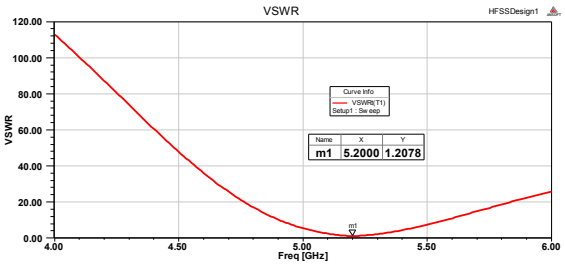

Fig. (22) VSWR for the proposed antenna at 5.2 GHz, ε_r=2.55

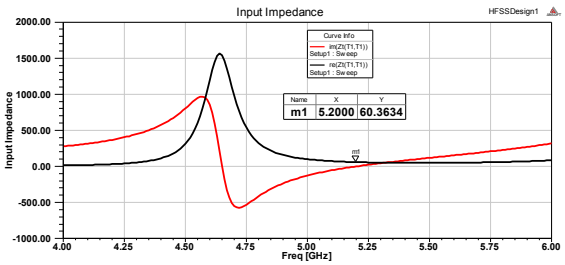

Fig. (23) Input Impedance for the proposed antenna at 5.2 GHz, ε_r=2.55

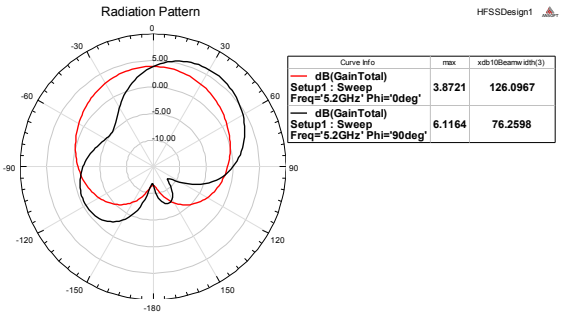

Fig. (24) 2D-Total gain for the proposed antenna at 5.2 GHz, ε_r=2.55

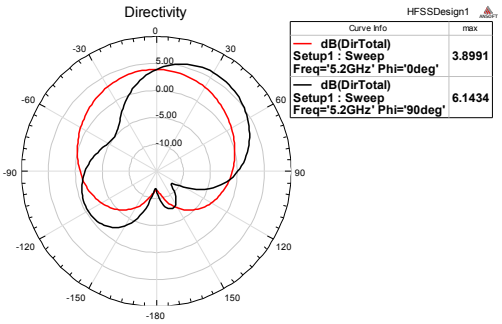

Fig. (25) 2D-Total Directivity for the proposed antenna at 5.2 GHz, ε_r=2.55

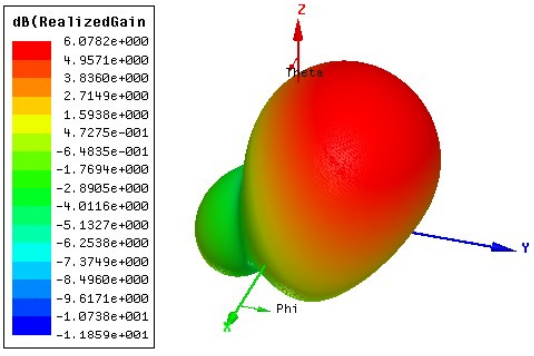

Fig. (26) 3D-Realized gain in dB for the proposed antenna at 5.2 GHz, ε_r=2.55

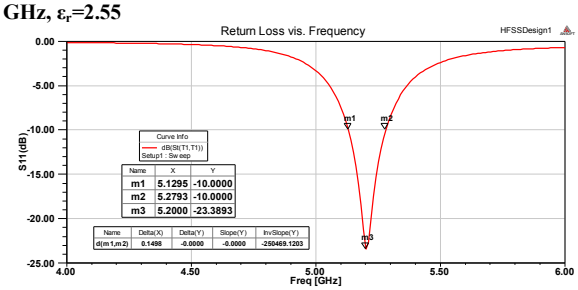

Fig. (27) Return Loss for the proposed antenna at 5.2 GHz, ε_r=3.2

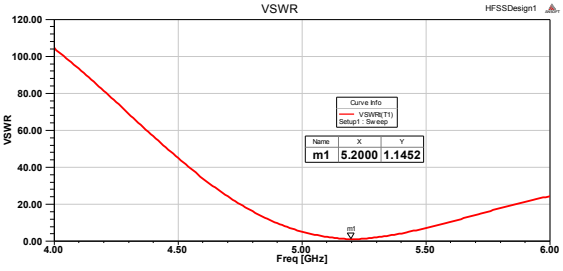

Fig. (28) VSWR for the proposed antenna at 5.2 GHz, ε_r=3.2

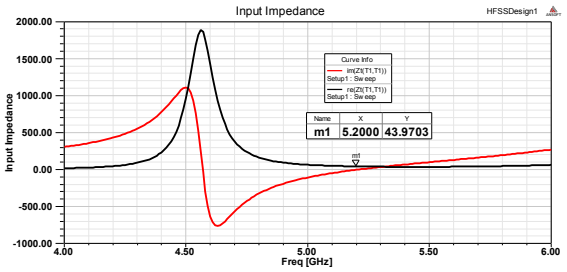

Fig. (29) Input Impedance for the proposed antenna at 5.2 GHz, ε_r=3.2

The radiation patterns shown in figures (30-32) confirm that the gain remains stable with broadside radiation maintained. Maximum achieved directivity stands at 6.2 dB, while maximum reached gain is 6.11 dB, which shows that the antenna maintains high radiation efficiency at this frequency, irrespective of the higher dielectric constant.

For ε_r = 4.4, the antenna resonance remains fixed at 5.2 GHz, with a return loss |S11| minimum of approximately −24.14 dB (Fig. 33), indicating a slight reduction in impedance matching quality. The voltage standing wave ratio reached to 1.13 (Fig. 34), while the input impedance is measured at 44.28 Ω (Fig. 35).

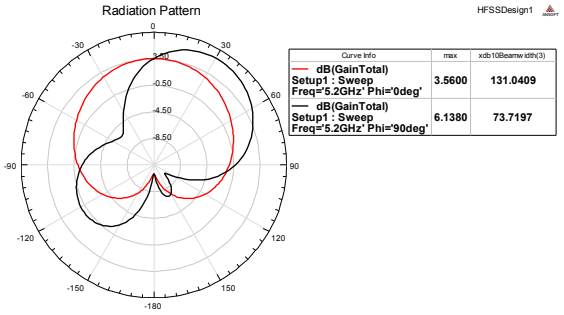

Fig. (30) 2D-Total gain for the proposed antenna at 5.2 GHz, ε_r=3.2

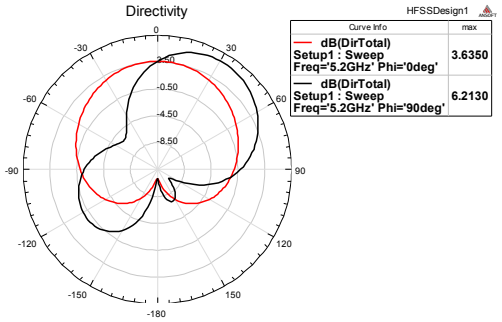

Fig. (31) 2D-Directivity for the proposed antenna at 5.2 GHz, ε_r=3.2

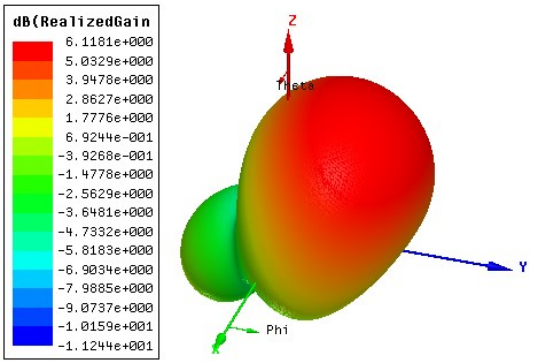

Fig. (32) 3D-Realized gain in dB for the proposed antenna at 5.2 GHz, ε_r=3.2

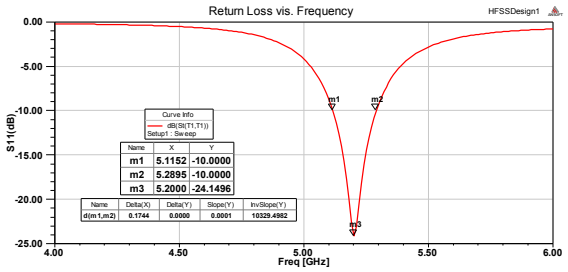

Fig. (33) Return Loss for the proposed antenna at 5.2 GHz, ε_r=4.4

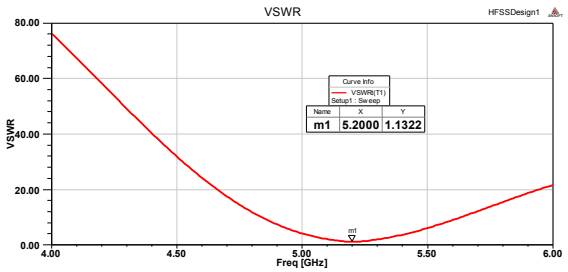

Fig. (34) VSWR for the proposed antenna at 5.2 GHz, ε_r=4.4

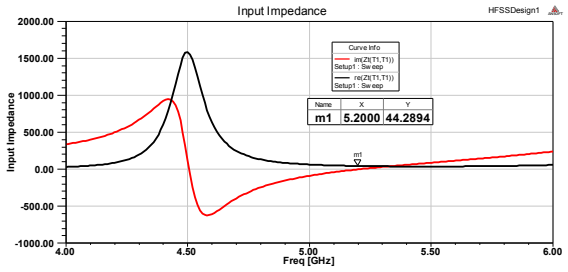

Fig. (35) Input impedance for the proposed antenna at 5.2 GHz, ε_r=4.4

Figures (36-38) present the radiation characteristics and confirm that the gain performance is consistent and a broadside radiation pattern is maintained. The maximum directivity obtained is 6.25 dB, whereas the peak gain reaches 4.62 dB, demonstrating efficient antenna operation at this frequency even for a higher dielectric constant.

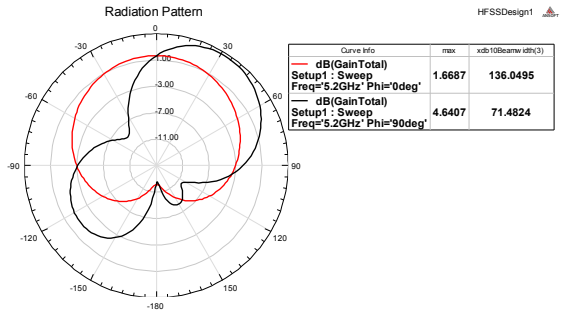

Fig. (36) 2D-Total gain for the proposed antenna at 5.2 GHz, ε_r=4.4

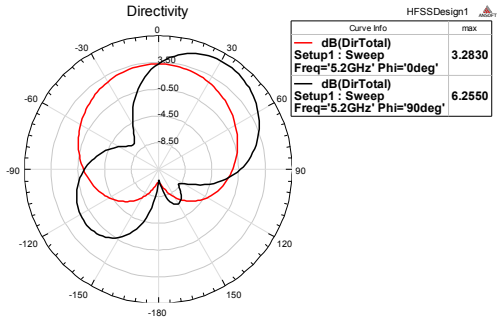

Fig. (37) 2D-Directivity for the proposed antenna at 5.2 GHz, ε_r=4.4

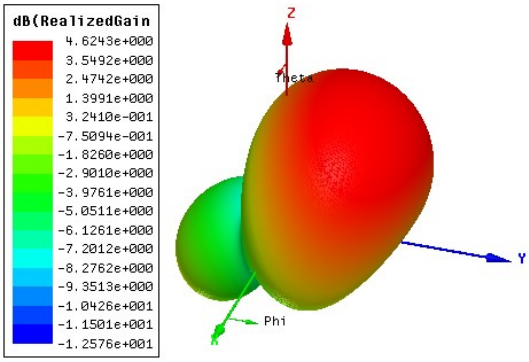

Fig. (38) 3D-Realized gain in dB for the proposed antenna at 5.2 GHz, ε_r=4.4

At 5.8 GHz, ε_r = 2.55, the return loss, as shown in Fig. (39), shows strong resonance at the same frequency with |S11| less than −21.37 dB, suggesting excellent impedance matching. As illustrated in Fig. (40), the VSWR at resonance is equal to 1.18. Input impedance at resonance is 59.28 Ω (Fig. 41).

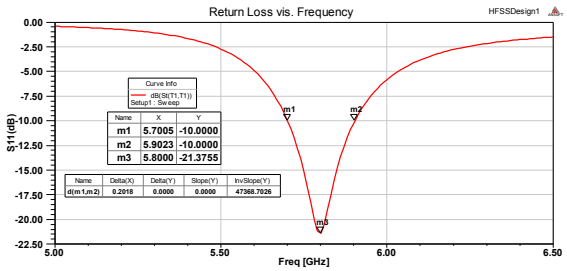

Fig. (39) Return loss for the proposed antenna at 5.8 GHz, ε_r=2.55

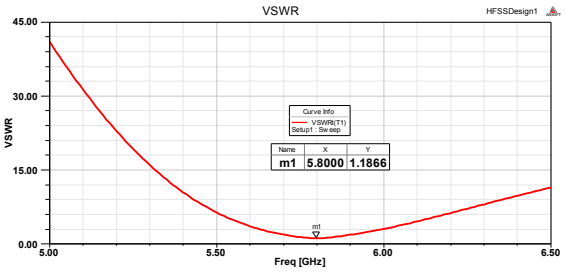

Fig. (40) VSWR for the proposed antenna at 5.8 GHz, ε_r=2.55

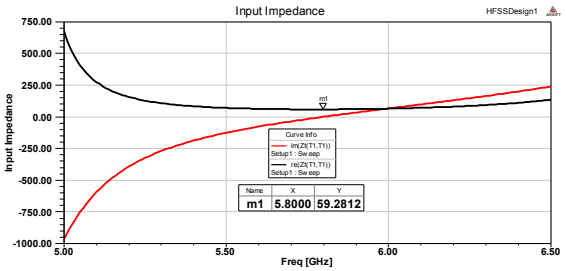

Fig. (41) Input impedance for the proposed antenna at 5.8 GHz, ε_r=2.55

Radiation characteristics (figures 42-44) indicate stable performance of the gain and a maintained broadside radiation pattern. The maximum directivity reached is 6.61 dB while the peak gain is 6.58 dB, hence, confirming that the antenna maintains high efficiency at this frequency.

With ε_r = 3.2, |S11| is -31.42 dB in Fig. (45), which means that resonance and impedance matching are good. The VSWR value corresponding to this is 1.05 as seen in Fig. (46), while the input impedance in Fig. (47) is 47.69 Ω.

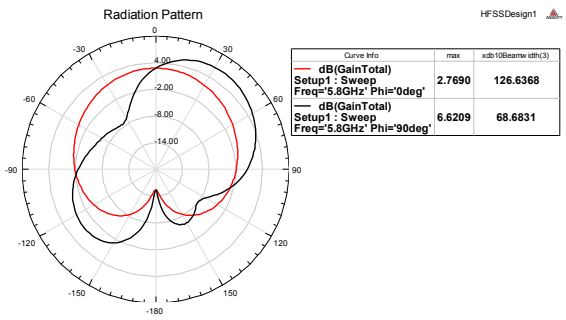

Fig. (42) 2D-Total gain for the proposed antenna at 5.8 GHz, ε_r=2.55

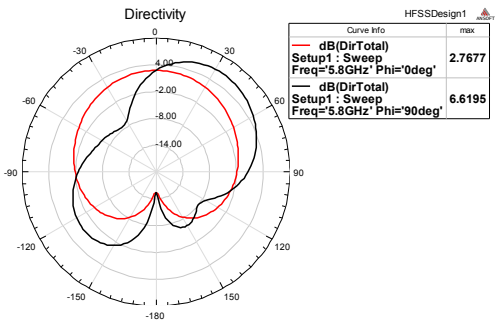

Fig. (43) 2D-Directivity for the proposed antenna at 5.8 GHz, ε_r=2.55

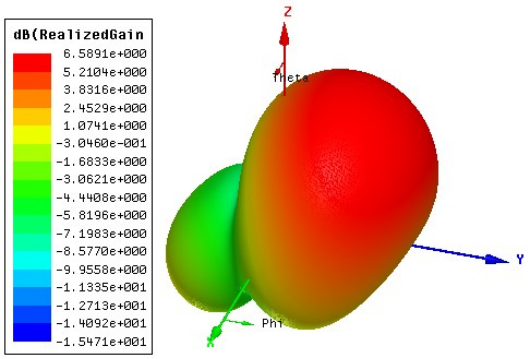

Fig. (44) 3D-Realized gain in dB for the proposed antenna at 5.8 GHz, ε_r=2.55

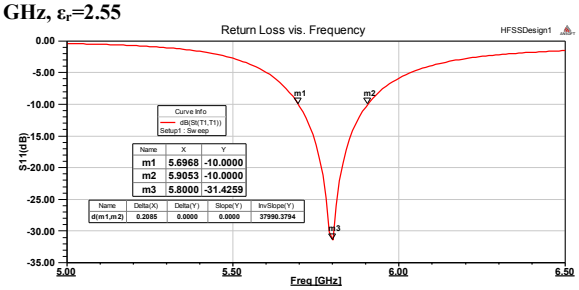

Fig. (45) Return Loss for the proposed antenna at 5.8 GHz, ε_r=3.2

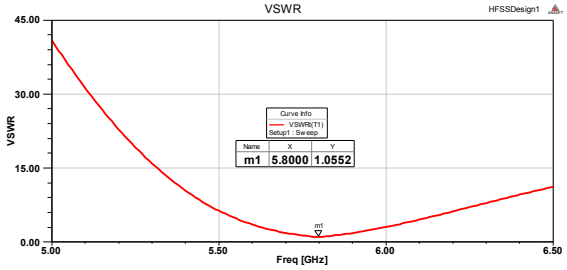

Fig. (46) VSWR for the proposed antenna at 5.8 GHz, ε_r=3.2

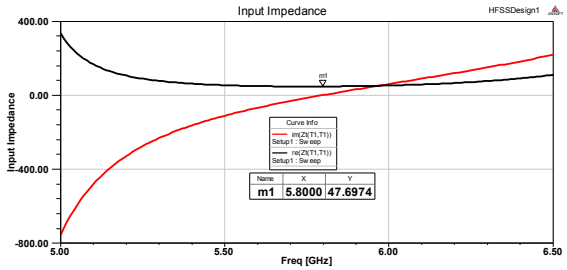

Fig. (47) Input Impedance for the proposed antenna at 5.8 GHz, ε_r=3.2

Figures (48-50) demonstrate the radiation characteristics that confirm stable gain performance with a broadside radiation pattern maintained. The maximum directivity achieved is 6.62 dB, while the peak gain reaches 6.57 dB, showing that the antenna maintains high efficiency at this frequency.

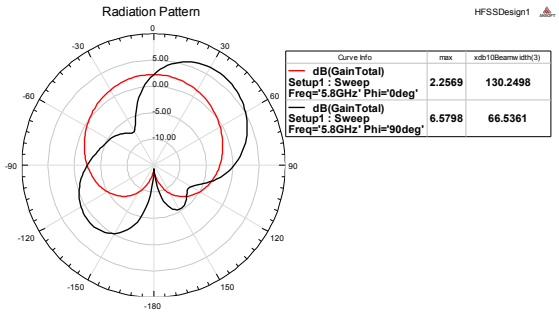

Fig. (48) 2D-Total gain for the proposed antenna at 5.8 GHz, ε_r=3.2

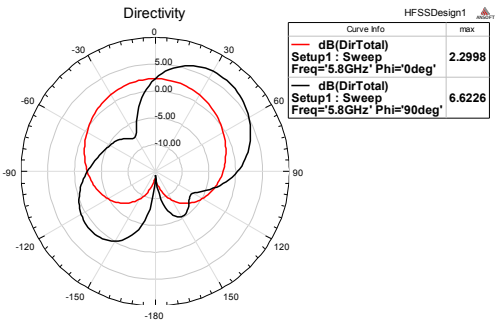

Fig. (49) 2D-Directivity for the proposed antenna at 5.8 GHz, ε_r=3.2

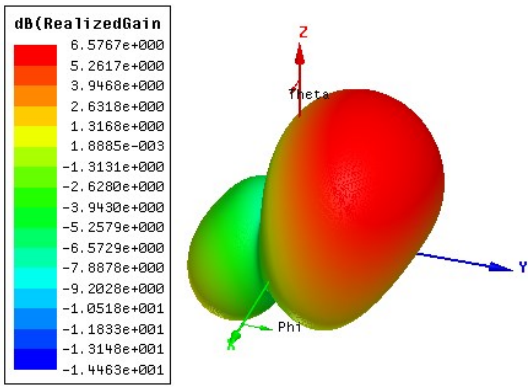

Fig. (50) 3D-Realized gain in dB for the proposed antenna at 5.8 GHz, ε_r=3.2

With ε_r = 4.4, the return loss is further enhanced as shown by Fig. (51) and |S11| ≈ −30.78 dB, which shows an excellent impedance matching while VSWR is 1.05 as obtained in Fig. (52) and input impedance of 47.28 Ω was measured from Fig. (53).

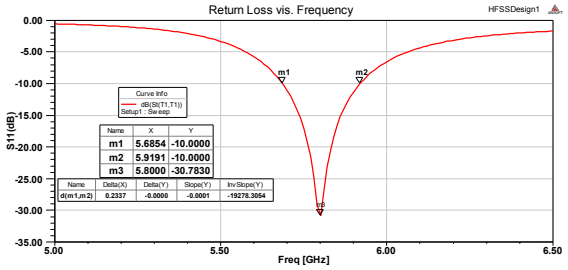

Fig. (51) Return Loss for the proposed antenna at 5.8 GHz, ε_r=4.4

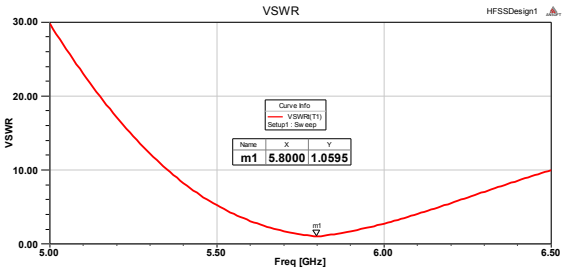

Fig. (52) VSWR for the proposed antenna at 5.8 GHz, ε_r=4.4

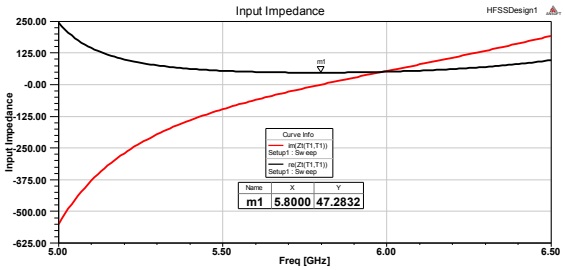

Fig. (53) Input Impedance for the proposed antenna at 5.8 GHz, ε_r=4.4

Figures (54-56) show that the radiation characteristics haves lightly reduced gain compared with lower-permittivity substrates, but with a broadside radiation pattern. The maximum directivity obtained is 6.5 dB and the peak gain reaches 5.32 dB, which confirms that the antenna continues to be highly efficient at this frequency. Analysis: At 5.8 GHz, the antenna operates efficiently across the studied range of permittivities, but the degradation with increased ε_r is sharper due to increased dielectric losses at higher frequencies.

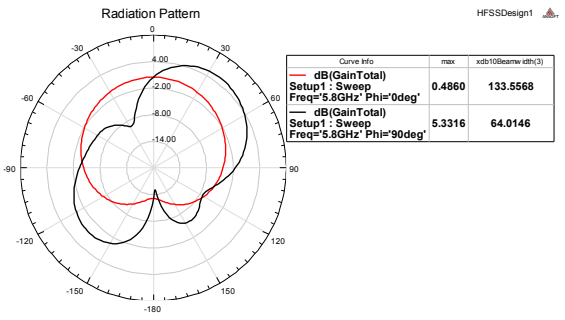

Fig. (54) 2D-Total gain for the proposed antenna at 5.8 GHz, ε_r=4.4

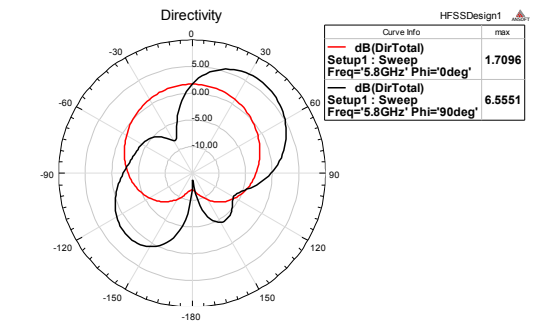

Fig. (55) 2D-Input Impedance for the proposed antenna at 5.8 GHz, ε_r=4.4

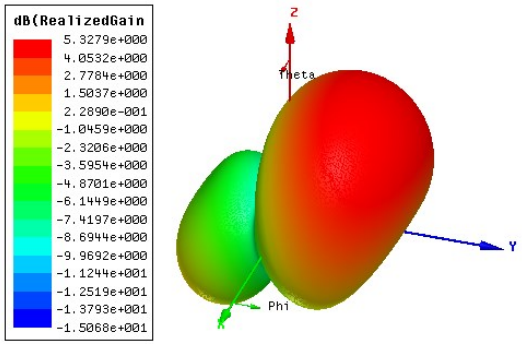

Fig. (56) 3D-Realized gain in dB for the proposed antenna at 5.8 GHz, ε_r=4.4

To highlight and discuss the results in detail, they will be summarized in table (2) as follows:

As shown in table (2), the simulated results of the semicircular PIFA antenna at 2.4, 5.2, and 5.8 GHz for different dielectric constants (ε_r = 2.55, 3.2, and 4.4) demonstrate the pronounced influence of both the substrate permittivity and frequency on the antenna's overall performance specifically on return loss, gain, radiation efficiency, impedance bandwidth, and the half-power beamwidths (HPBW) in the E- and H-planes. The data reveal distinct electromagnetic behavior trends that clarify the physical mechanisms governing the antenna's response.

At the frequency of 2.4 GHz, the radiation characteristics degrade with an increase in substrate relative permittivity; that is, the gain reduces from 5.26 dB at ε_r = 2.55 to 3.01 dB at ε_r = 4.4, and the radiation efficiency reduces greatly from 0.99 to 0.60. This phenomenon can be attributed mainly to the increased surface wave characteristics of the substrate with higher relative permittivity. These surface waves increase the confinement of the electromagnetic fields within the substrate and result in higher losses of the material due to the confined electromagnetic fields. This reduces the power that can be radiated into the free space. The impedance bandwidth improves slightly from 57.6 MHz at ε_r = 2.55 to 84.6 MHz at ε_r = 4.4. This increase in the impedance bandwidth may be attributed to the fact that the antennas designed on the higher relative permittivity substrate result in higher frequency band performance because of better impedance matching and higher parasitic capacitance. A higher relative permittivity of the substrate results in reduced fringing fields with increased capacitive effects. As a result of this increased impedance bandwidth, the efficiency of the radiated fields reduces.

At the higher frequency ranges of 5.2 GHz and 5.8 GHz, the gain values of the antenna are found to remain higher when substrates with ε_r = 2.55 and 3.2 are used. However, there is a reduction in the gain as well as the efficiency of radiation when ε_r = 4.4 due to the increased effects of dielectric losses on the

electromagnetic characteristics. For this substrate, the radiation efficiency decreases from approximately 0.99 to 0.74 at 5.2 GHz and from 0.99 to 0.81 at 5.8 GHz. This reduction is consistent with the well-established behavior of printed antennas, where higher permittivity enhances energy confinement within the dielectric and consequently diminishes radiated power. Even with these losses, all types of substrates still show an overall increase in gain with frequency. At higher frequencies, radiation directivity improves because shorter wavelengths make radiation patterns more focused.

The values of the VSWR, ranging from 1.07 to 1.23 at their respective resonance points, clearly identify that the impedance characteristics of the designed antenna remain excellent throughout the tested operating frequencies. The impedance band width widens significantly with an increase in frequency; that is, the width varies from 57.6 MHz at the frequency of 2.4 GHz to 201.8 MHz at the frequency of 5.8 GHz. This identifies that the quality factor (Q) reduces with an increase in the frequency of the radiator because of the relatively low stored reactive power at higher frequencies.

The radiation pattern displays strong stability over the frequency band. The half-power beam width (HPBW) of the E-plane ranges between 119° and 140° at 2.4 GHz frequency but remains within the limits of 126°-133° at higher frequencies. On the other hand, the value of the H-plane HPBW reduces systematically from around 97° at 2.4 GHz frequency to about 64° at 5.8 GHz frequency. This measured reduction of the width definitely adds up to the measured increase of the directivity value. Keeping this enhancement of directivity in mind, the designed antenna still supports broad coverage area with sufficient width on the principal planes; thus, the designed antenna works well with the short-range communication system like Wi-Fi and Bluetooth that necessitates relatively uniform behavior of the omni-direction pattern.

The relationship between gain, directivity, and efficiency of radiation follows the conventional form given by the equation $\eta = G/D$ [22]. This is illustrated at a frequency of 2.4 GHz with $\varepsilon_r = 4.4$; a gain of 3.01 dB and directivity of 5.00 dB result in an efficiency of about 0.60. The very close agreement between the theoretical calculation and the HFSS solution confirms that the computational methodology employed is accurate and that the choice of the boundary conditions used during the simulation is adequate.

On the whole, the above results show that the higher the substrate permittivity, the poorer the radiation performance because of the increased dielectric loss and the higher probability of surface wave excitation. On the other hand, the higher frequency of operation improves the directivity and gain of the antenna as well as its HPBW, thereby improving the radiation performance at the higher frequency ranges. The semicircular PIFA therefore supports a stable impedance response, predictable radiation patterns, and reasonably efficient performance over the entire set of design options, making it an excellent contender for compact multiband wireless communication systems. A substrate with 'moderate' values of ε_r between 2.55 and 3.2 supports the best compromise between efficiency and gain performance with predictable radiation patterns. Although higher-permittivity materials like FR4 with $\varepsilon_r = 4.4$ remain relatively low in cost and readily accessible, higher losses due to the dominant dielectric and surface wave effects undermine the efficiency of the radiation process and are therefore not desirable for advanced multiband antenna designs operating within the frequency band of 2.4-5.8 GHz.

Following the HFSS simulations, the semicircular PIFA antenna with a dielectric constant of $\varepsilon_r = 4.4$ was selected for fabrication due to the availability of this substrate material in the laboratory. The antenna prototypes were manufactured for the targeted frequencies of 2.4, 5.2, and 5.8 GHz (Fig. 57). Experimental measurements were performed on the fabricated prototypes, and the results were compared with the simulated data. The measured return loss curves (figures 58-60) indicate resonances closely aligned with the designed frequencies, with minor frequency shifts observed. These deviations are attributed to fabrication tolerances, conductor parasitic effects, and slight variations in the actual dielectric constant of the FR4 substrate. Overall, the strong correlation between simulation and measurement validates the proposed semi-empirical radius formula and demonstrates the feasibility and effectiveness of the semicircular PIFA design.

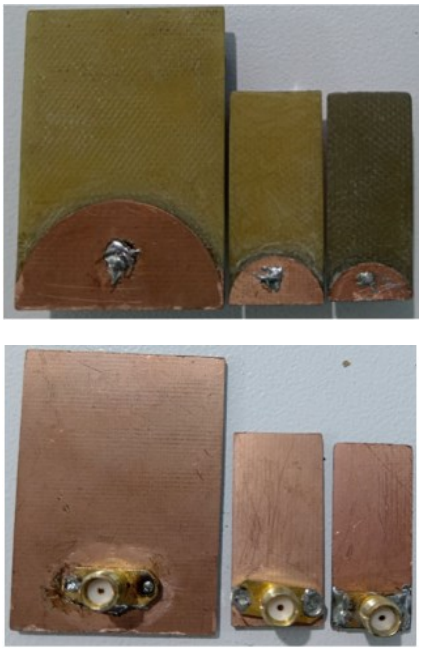

Fig. (57) Upper and lower faces of the manufactured PIFAs

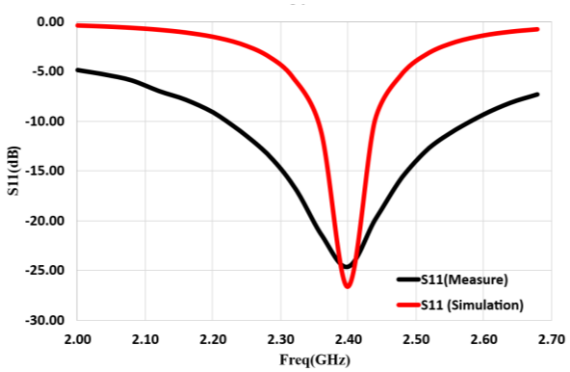

Fig. (58) Comparison between the theoretical and experimental results for the S11 reflection coefficient at 2.4 GHz, ε_r=4.4

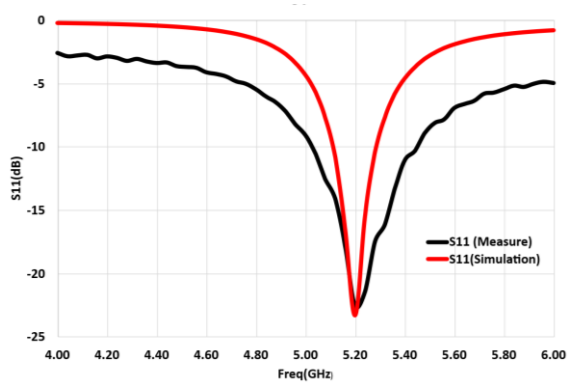

Fig. (59) Comparison between the theoretical and experimental results for the S11 reflection coefficient at 5.2 GHz, ε_r=4.4

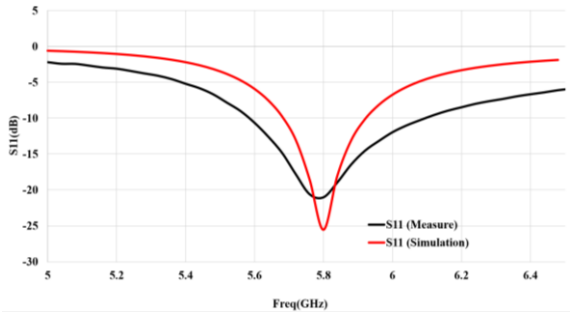

Fig. (60) Comparison between the theoretical and experimental results for the S11 reflection coefficient at 5.8 GHz, ε_r=4.4

Additional comparisons were performed across a range of frequencies and dielectric constants to improve the study and guarantee the validity of the semi-empirical equation in a variety of real-world situations. The numbers obtained from the circular shape Eq. (1) were found to be extremely close to the values obtained from the semi-empirical Eq. (8), which equates the surface area of a semicircle to that of a rectangle. As indicated in table 3 below, where X stands for Eq. (8), while Y for Eq. (1), there is a significant correlation between the computed values derived from Eq. (8) and Eq. (1) for the radius of the semi-circle and circular patch antenna. The values of the arithmetic mean, standard deviation, coefficient of variation, and Pearson's correlation coefficient are displayed in table (3). It turns out that the standard deviation, which gauges how far values deviate from the arithmetic mean, is extremely low. In the same way, the coefficient of variation, which is the ratio of the standard deviation to the arithmetic mean and serves as a relative indicator of dispersion, is likewise minimal. Pearson's correlation coefficient, which measured the extent to which two variables are related, is near +1. There is a significant direct association between variables X and Y which is suggested by this closeness to +1, which indicates a strong positive correlation.

4. Conclusion

The results obtained in this work confirm the equation proposed here as a precise and reliable way to calculate the radius of semicircular PIFA antennas. In fact, theoretical predictions are in good agreement with HFSS simulations and the experimental measurements, of various frequencies and substrate materials, showing the robustness and wide applicability of the model. The correlation coefficient was also very high, further validating that the equation could usefully guide practical antenna design. This equation simplifies the process of optimizing semicircular geometries for researchers and engineers with a high degree of accuracy, which will help ensure better performance of compact wireless communication devices.

References

[1] M. Rawat and V.V. Thakare, "Multiband PIFA Antenna for Mobile Applications", in *2024 2nd World Conf. Communicat. Comput. (WCONF)*, IEEE (2024), pp. 1-9.

[2] M.I. Hossain, M.R.I. Faruque and M.T. Islam, "Analysis on the effect of the distances and inclination angles between human head and mobile phone on SAR", *Prog. Biophys. Mol. Biol.*, 119(2) (2015) 103-110.

[3] H. Ben Hamadi et al., "Analysis and design of a new PIFA antenna for the wireless communications applications," in *2019 IEEE 19th Mediterranean Microwave Symp. (MMS)*, IEEE (2019), pp. 1-4.

[4] K.H. Chan et al., "Effect of internal patch antenna ground plane on SAR", in *2006 17th Int. Zurich Symp. Electromag. Compatib.*, IEEE, 2006, pp. 513-516.

[5] L. Wakrim et al., "Novel design of a triple band PIFA antenna by using a binary genetic algorithm", *J. Comput. Electron.*, 20 (2021) 1373-1386.

[6] A.K. Penta and C.R.P. Kumar, "A Novel PIFA Design for SAR Reduction in 5G Networks to Analyze the RF Shield Impact", *Eng. Technol. Appl. Sci. Res.*, 14(3) (2024) 14102-14108.

[7] G.A. Ahmed and A.H. Sallomi, "SAR Calculation in a Child Seven-Layer Head Model at 2.1 and 2.6 GHz", *Wasit J. Comput. Math. Sci.*, 2(1) (2023) 40-45.

[8] J. Keshvari et al., "Large scale study on the variation

of RF energy absorption in the head & brain regions of adults and children and evaluation of the SAM phantom conservativeness", *Phys. Med. Biol.*, 61(8) (2016) 2991.
[9] M.R. Iqbal-Faruque et al., "Effects of mobile phone radiation onto human head with variation of holding cheek and tilt positions", *J. Appl. Res. Technol.*, 12(5) (2014) 871-876.
[10] A. Lak, N. Parhizgar and M. Lak, "Effect of presence of human body on antenna gain", *Indian J. Sci. Technol.*, 8(30) (2015) 1-8.
[11] S.S. Pudipeddi and P.V.Y. Jayasree, "Investigation of the Effect of Normal Incidence of RF Wave on Human Head Tissues Employing Cu and Ni Grid PET Films", *Eng. Technol. Appl. Sci. Res.*, 12(6) (2022) 9445-9449.
[12] S.K. Koul and G.S. Karthikeya, **"Antenna Architectures for Future Wireless Devices"**, Springer (2021).
[13] K. Fujimoto, **"Mobile Antenna Systems Handbook"**, Artech House (2008).
[14] K. Hirasawa, **"Analysis, Design, and Measurement of Small and Low-Profile Antennas"**, Artech House (1992).
[15] R. Kaur and D. Khosla, "Study of Planar Inverted-F Antenna Structures for Various", *Int. J. Electr. Electron. Eng.*, 2(3) (2015) 24-26.
[16] P. Song et al., "Triple-band planar inverted F antenna", in *IEEE Antennas Propag. Soc. Int. Symp.*, IEEE (1999), pp. 908-911.
[17] P. Ciais et al., "Compact internal multiband antenna for mobile phone and WLAN standards", *Electron. Lett.*, 40(15) (2004) 1.
[18] H. Mishima and T. Taga, "Mobile antennas and duplexer for 800 MHz band mobile telephone system", in *1980 Antennas Propag. Soc. Int. Symp.*, IEEE (1980), pp. 508-511.
[19] M.H. Tsoi and S.W.Y. Mung, "Planar antenna design for internet of things applications", in *Advanced Radio Frequency Antennas for Modern Communication and Medical Systems*, IntechOpen (2020).
[20] S.K. Ghosh et al., "Probe-fed semi circular microstrip antenna vis-à-vis circular microstrip antenna: a necessary revisit", in *IOP Conf. Ser.: Mater. Sci. Eng.,* IOP Publishing (2018), 12026.
[21] K.P. Ray and G. Kumar, "Determination of the resonant frequency of microstrip antennas", *Microwave Opt. Technol. Lett.*, 23(2) (1999) 114-117.
[22] C.A. Balanis, **"Antenna Theory Analysis and Design"**, 3rd ed., John Wiley & Sons (NY, 2005).
[23] R. Waterhouse, **"Microstrip patch antennas," in Handbook of Antennas in Wireless Communications"**, CRC Press (2018), pp. 1-6.
[24] A.I.P. Bhartia et al., **"Microstrip Antenna Design Handbook"**, Artech House (2001).
[25] G. Kumar and K.P. Ray, **"Broadband Microstrip Antennas"**, Artech House (MA, 2016).
[26] I.N. Taban, A.H. Khidhir and A.A. Naser, "Design and Simulation of Planar Inverted F Antenna (PIFA) for Long Term Evolution Systems", *Al-Nahrain J. Sci.*, 25(4) (2022) 43-48.
[27] S.D. Mallanna, K. Viswanath and P.K.B. Rangaiah, "Design and Analysis of High Gain Planar Inverted-F Antenna (PIFA) for Wimax and Nomadic Applications," in *2021 Int. Conf. Wireless Communicat. Signal Process. Network. (WiSPNET 2021)*, IEEE (2021), pp. 6-10.

Table (1) Variation of antenna radii with frequency and dielectric constants

h (mm)	l_g (mm)	f (GHz)	ε_r	r (mm)	w_g (mm)	w_s (mm)
1.6	**50**	**2.4**	2.55	22.03	44.06	44.06
			3.2	20.02	40.04	40.04
			4.4	17.40	34.80	34.80
1.6	**35**	**5.2**	2.55	19.16	19.36	19.36
			3.2	8.92	17.84	17.84
			4.4	7.92	15.84	15.84
1.6		**5.8**	2.55	8.70	17.42	17.42
			3.2	8.04	16.08	16.08
			4.4	7.16	14.32	14.32

Table (2) Simulated performance parameters of the semicircular PIFA antenna at different frequencies and dielectric constant

f (GHz)	ε_r	S_{11} (dB)	Gain (dB)	Directivity (dB)	Radiation Efficiency	Input Impedance (Ω)	VSWR	Bandwidth (-10 dB, MHz)	HPBW(E)^0	HPBW(H)^0
2.4	2.55	-19.8	5.258	5.307	0.99	52.3	1.22	57.6	119.79	97.18
	3.2	-26.26	5.047	5.176	0.97	46.72	1.10	63.5	127.47	95.70
	4.4	-26.66	3.011	5.004	0.60	46.5	1.09	84.6	140.06	93.63
5.2	2.55	-19.47	6.078	6.143	0.99	61.8	1.23	143.3	126.09	76.25
	3.2	-22.84	6.118	6.213	0.98	43.37	1.15	149.8	131.04	73.71
	4.4	-23.29	4.624	6.255	0.74	43.59	1.14	174.4	136.04	71.48
5.8	2.55	-20.65	6.589	6.619	0.99	60.18	1.20	201.8	126.63	68.68
	3.2	-28.62	6.576	6.622	0.99	46.42	1.07	208.5	130.24	66.53
	4.4	-25.52	5.327	6.555	0.81	45.01	1.11	233.7	133.55	64.01

Table (3) Central tendency and linear regression measurements results

F	2.4 GHz			3.2 GHz			5.2 GHz			5.8 GHz	
ε_r	X	Y		X	Y		X	Y		X	Y
2.55	22.02	22.033		16.352	15.978		9.849	9.685		8.78	8.715
3.2	19.756	20.019		14.689	14.598		8.872	8.927		7.914	8.049
3.78	18.238	18.617		13.571	13.631		8.211	8.393		7.328	7.58
4	17.748	18.157		13.210	13.313		7.997	8.217		7.138	7.424
4.4	16.951	17.400		12.622	12.79		7.648	7.926		6.829	7.168
5.5	15.217	15.725		11.342	11.627		6.886	7.277		6.151	6.596
6	14.589	15.110		10.877	11.198		6.601	7.036		5.904	6.383
Mean	17.78	18.15		13.23	13.30		8.00	8.20		7.14	7.41
S.D	2.56	2.39		1.89	1.65		1.12	0.91		0.99	0.80
CV%	14.42	13.20		14.28	12.44		14.00	11.18		13.90	10.89
R		**0.99979**			**0.99975**			**0.99976**			**0.99972**

